Applied Thermal Engineering 60 (2013) 411–422

Contents lists available at ScienceDirect

Applied Thermal Engineering

journal homepage: www.elsevier.com/locate/apthermeng

Research paper

The experimental validation of a transient power electronic building block (PEBB) mathematical model

E. Dilay [a], J.V.C. Vargas [a,*], J.C. Ordonez [a], S. Yang [a], R. Schrattenecker [a], M. Coleman [a], T. Chiocchio [a], J. Chalfant [b], C. Chryssostomidis [b]

[a] Department of Mechanical Engineering and Center for Advanced Power Systems, Florida State University, Tallahassee, FL 32310, USA
[b] MIT Sea Grant Design Laboratory, Massachusetts Institute of Technology, Cambridge, MA 02139, USA

HIGHLIGHTS

- We amended and tested a general computational model for electronic packages.
- Experimental and numerical results are in good quantitative and qualitative agreement.
- A transient simulation study was conducted with the model.
- The system thermal conductance was determined and investigated.
- Model could be a tool for simulation, design, and optimization of electronic packages.

ARTICLE INFO

Article history:
Received 15 May 2013
Accepted 3 July 2013
Available online 12 July 2013

Keywords:
vemESRDC
Mesh generation
Thermal management
Early stage design tool
Heat transfer

ABSTRACT

This work adjusts and validates experimentally a previously developed volume element model based thermal management tool (vemESRDC) through the comparison of temperature measurements of a power electronic building block (PEBB) to numerical simulation results, featuring relevant electronic components of an all-electric ship. Primary components of interest in this simulation are: inductors, capacitors, AC and DC fuses, and a tiristors/fins set. The vemESRDC is a thermal simulation tool developed as part of the Electric Ship Research and Development Consortium (ESRDC) funded by the Office of Naval Research (ONR) that is capable of providing quick responses during early stages of ship design. The model adjustment was conducted by solving the inverse problem of parameter estimation for appropriate equipment properties using a total power dissipation of 4.8 kW in the PEBB. Next, the adjusted model was experimentally validated using the same PEBB with a power dissipation of 11.12 kW. The transient and steady state numerical results are shown to be in good quantitative and qualitative agreement with the experimental measurements within the experimental error margin. Transient simulations demonstrate that the components temperature vary significantly from one heating mode to another, whereas internal air average temperature varies only slightly for all heating modes, therefore not only average internal air temperature should be monitored for preserving equipment functionality. As a result, it is expected that vemESRDC could be used as a reliable tool for transient and steady state thermal management of heat generating packages (e.g., PEBB, future all-electric ship).

1. Introduction

The so called all-electric ship is expected to make more efficient use of on-board power and to cut fuel use, so that future requirements for high-power weapons such as the electromagnetic gun, high power microwave and high energy lasers could be met. The US Navy's Office of Naval Research (ONR) created five "focus areas" for the development of the all-electric ship: i) power generation; ii) distribution and control; iii) energy storage; iv) heat transfer and thermal management; and v) motors and actuators, as reported by Wagner [1], which are highly interdependent for synchronized and optimal operation. Therefore unexpected performance and failure of mechanical-electrical systems to the detriment of the ship's combat mission could result from poor thermal management [2].

Reliable thermal models are crucial for all-electric ship design, so that thermal management could be optimized for maximum

* Corresponding author. Tel.: +1 850 644 8405; fax: +1 850 645 1534.
E-mail addresses: jvargas@caps.fsu.edu, vargasjvcv@gmail.com (J.V.C. Vargas).

1359-4311/$ – see front matter © 2013 Elsevier Ltd. All rights reserved.
http://dx.doi.org/10.1016/j.applthermaleng.2013.07.005

Nomenclature

A	area, m^2
B_a	bias limit of quantity a
c	specific heat, J kg^{-1} K^{-1}
IPPE	inverse problem of parameter estimation
k	thermal conductivity, W m^{-1} K^{-1}
L	length, m
m	mass, kg
$\dot{m}$	mass flow rate, kg s^{-1}
N	total number of volume elements
ONR	office of naval research
p_v	vapor pressure, N m^{-2}
p_{vs}	water saturation pressure, N m^{-2}
P_a	precision limit of quantity a
PEBB	power electronic building block
$\dot{Q}$	heat transfer rate, W
S	heat transfer surface, m^2
t	time, s
T	temperature, K
U	global heat transfer coefficient, W m^{-2} K^{-1}
U_a	uncertainty of quantity a
UA	global thermal conductance, W K^{-1}
v	velocity, m s^{-1}
vemESRDC	volume element based thermal management tool
V	volume, m^3
VE	volume element
VEM	volume element model
x, y, z	Cartesian coordinates, m

Greek letters

γ	heat transfer surfaces ratio
ΔT	temperature difference, K
ε	relative error
ρ	density, kg m^{-3}
σ	standard deviation
φ	relative humidity

Subscripts

air	internal air
avg	average
co	component
conv	convection
e	east
eq	equivalent
f	fluid
fan	fan
free	free cross flow
gen	generation
i	volume element number
in	inlet
j	volume element face
m	mesh
max	maximum
n	north
p	gas at constant pressure
R	actual
s	south
t	top
tot	total
v	gas at constant volume
w	west
x	x-direction
y	y-direction
z	z-direction
0	initial condition
∞	external air
$\lvert \cdot \rvert$	absolute value
$\lVert \cdot \rVert$	Euclidean norm

global system efficiency. As electronic devices integrated for control, power, and propulsion systems dissipate noticeable amount of heat, the all-electric ship's performance is heavily dependent on large thermal transients. Improper thermal management usually results in thermal runaway of electronic devices, leading to system failure. Thus, concrete component-level thermal management strategies must be developed in order to prevent potential system faults and satisfy cooling requirements.

Recent studies [3,4] state that process integration, which is a key enabler to increasing efficiency in energy generation industries, leads to increasingly complex dynamic behavior, such that tightly integrated designs continue to be regarded with caution owing to the dynamics and control difficulties that they pose. This complexity demands simple and computationally fast component models which can be combined to produce the global system response.

Thermo-mechanical stresses are known to damage electronics equipment, and could only be accessed through the knowledge of the equipment and surroundings temperature field. Therefore methodologies to trigger repair or replacement, significantly prior to failure are needed, and several approaches have been proposed with the finite element method (FEM), or even non-linear least-squares method based on interrogation techniques, so that it was possible to calculate the prior damage in electronics subjected to cyclic and isothermal thermo-mechanical loads [5–7]. Bagnoli et al. [8] proposed an analytical thermal solver to replace the onerous programs based on the FEM, but applied the strategy only to steady state two-layer virtual structures and compared to published FEM results. Yang and Chen [9] conducted an experimental investigation for testing dynamic behavior of plastic ball grid array (PBGA) integrity in electronic packaging, but considered only fixed modes for design and reliability evaluation, and emphasized the need for accurate mathematical modeling and low time-consuming computer applications. The main message from all these studies is that the electronic system packaging community has a great need to reduce the size of its heat transfer simulations.

Shapiro [10] presented an overview on existing models of complex electronic systems, and proposed the creation of compact models to address the problem. The author states that "for system design, small not-so-accurate models are more useful than large accurate models", and concludes that the strategies to achieve that goal could be model reduction and experimental identification, so that heat transfer simulations size reduction would be obtained, and should also benefit from empirical correlations for complex situations (e.g., turbulent flows through complex geometries).

The thermal response of electronic packages and all-electric ships has been investigated through a simplified physical model in previous studies [11–14]. A comprehensive computational visualization tool has also been added to the model to obtain total solutions to thermal and electrical management [15,16]. In this way, visualization that geographically lays out the integrated system's critical thermal management systems and addresses adaptive control issues in a system context has been made possible. These efforts resulted in the development of a volume element model

based thermal management tool (vemESRDC) [17] that combines conservation principles with empirical correlations, and presents low computational time requirements both for transient and steady state analyses. However, in order to use the model to develop concrete component-level thermal management control strategies for maximum global system performance, model experimental validation is a mandatory step.

The bibliographic review points to the need of sufficiently accurate, and low time consuming compact models for electronics packaging. As a result, the objective of this study is to adjust and validate experimentally the tool vemESRDC through the comparison of temperature measurements of power electronic building blocks (PEBB) to numerical simulation results, featuring relevant electronic components of a future all-electric ship. The analysis is conducted both for the transient and steady state regimes.

2. Theory

This work is part of a larger effort to produce an adequate tool to provide quick responses during early stages of ship design. Therefore a simplified mathematical model was devised to simulate a notional all-electric ship thermal behavior both in transient and steady-state regimes. However, since the ship was treated as a system with generic boundaries, which is allowed to interact dynamically with the surroundings, it is reasonable to state the model could be used for the thermal analysis of any similar system.

The problem consists of computing the system temperature and relative humidity distributions. These distributions are determined by external environmental conditions, and by the geometrical distribution of the internal components, which in addition, can generate heat. The internal temperature and relative humidity internally should not exceed the components and internal compartments desired operating conditions.

Although the ship complex integrated system operating dynamically or at steady state has been presented by the authors before [12–14,17], modifications have been introduced in this work in order to allow for mass flow across the boundaries. Hence, in order to provide a clear understanding of the model and the experimental validation procedure, it is instructive to summarize its main features together with the new aspects.

The main objective of the model is to obtain accurate temperature and relative humidity distributions, whenever forced convection is present, thus the required flow field in the domain is imposed approximately, based on the knowledge of external environmental conditions (e.g., wind and sea water speed) and internal components (e.g., mass flow rates, fans, turbines). Therefore, the governing equations are only the mass and energy conservation principles applied to each volume element, VE, which consists of a brick with 6 planar faces. A mesh is built with such volume elements to represent the entire region of interest to be analyzed (e.g., the whole ship, a power electronic building block).

The combination of the proposed simplified physical model with the adopted finite volume scheme for the numerical discretization of the differential equations is called a volume element model (VEM) [11]. The model takes into account the existence of element internal heat sinks (or sources) and the heat and mass transfer processes through the six element faces, by conduction, convection and radiation (e.g., sun incidence on the domain boundaries).

Fig. 1 shows a typical cell (or volume element) that may contain either fluid and/or solid material, according to the element type. Each element interacts with the other adjacent elements, and with the environment if located in the system boundaries, according to the energy equation (first law of thermodynamics) applied to the cell, as follows:

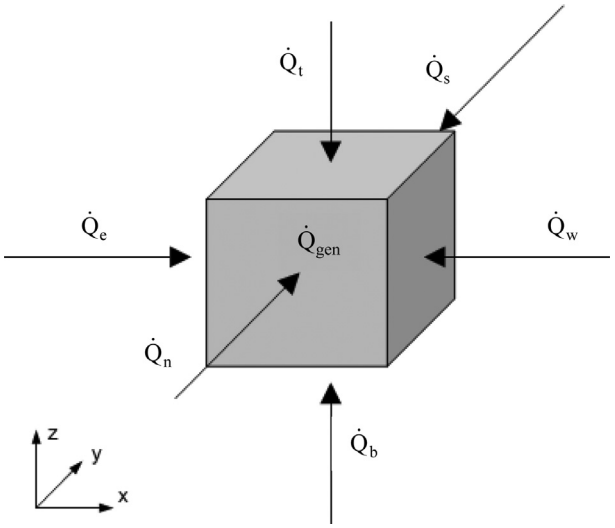

Fig. 1. Mesh volume element (VE) with heat transfer interactions.

$$\frac{dT_i}{dt} = \frac{1}{(\rho\, V\, c)_i}\left(\sum_{j=e,w,t,b,n,s} \dot{Q}_j + \dot{Q}_{gen} + \dot{Q}_{conv}\right)_i \tag{1}$$

where $1 \le i \le N$, with N being the total number of elements in the mesh, T_i are the temperatures of each volume element, ρ is the density of the material inside the volume element (fluid and/or solid), V is the total cell volume, c is either the specific heat of the solid/liquid or the specific heat at constant volume of the gas inside the volume element (c_v), $\dot{Q}_e$, $\dot{Q}_w$, $\dot{Q}_t$, $\dot{Q}_b$, $\dot{Q}_n$, $\dot{Q}_s$ and $\dot{Q}_{gen}$ are the heat transfer rates (by conduction, convection and radiation) across the east, west, top, bottom, north, south faces of each volume element and the heat sink or source inside the element, respectively, and $\dot{Q}_{conv}$ is the net heat transfer rate collected/rejected through convection by one or more fluid streams (cooling fluids, e.g., fresh or sea water) that flow through the volume element.

The system of ordinary differential equations defined by Eq. (1) formulates the initial value problem to be solved, depicting the temperature field inside the integrated system at any instant of time, for given initial conditions T_{i0}.

Next, the relative humidity at each air element (relative humidity field) follows from the temperature field, by assuming a known initial relative humidity condition, φ_{i0}. First, the initial vapor pressure is calculated as follows:

$$p_{v,i} = \varphi_{i0} \cdot p_{vs}(T_{i0}) \tag{2}$$

where $p_{v,i}$ is the cell partial vapor pressure, φ_{i0} is the cell initial relative humidity, $p_{vs}(T_{i0})$ is the water saturation pressure at T_{i0}.

It is assumed that the absolute humidity in each volume element remains approximately constant during the entire simulation. Hence, the relative humidity at each element that contains air is computed from

$$\varphi_i = \frac{p_{v,i}}{p_{vs}(T_i)} \tag{3}$$

where φ_i is the relative humidity of the cell and $p_{vs}(T_i)$ is the water saturation pressure at temperature T_i. When the element contains solid equipment (or liquids) a zero value is assigned to it, i.e., $\varphi_i = 0$.

The mathematical model was originally written for treating the notional all-electric ship as an enclosure, i.e., a closed system. So, the

different integrated system components and their cooling strategies comprised 6 (six) volume element types that were defined based on their contents: 0) only air; 1) pure solid; 2) compact heat exchanger; 3) chilled fluid units; 4) internal fluid (closed loop) cooled systems, and 5) external fluid (open loop) cooled systems. Therefore, for treating one component in isolation, such as the PEBB, that is allowed to be crossed by a cooling mass flow through the external boundaries (e.g., external air cooling flow induced by a fan), an additional volume element type was defined, i.e., 6) cooling fluid flowing through the element, so that the heat transfer rate through convection for VE i, $\dot{Q}_{conv,i}$, is calculated as follows:

$$\dot{Q}_{conv,i} = \dot{m}_i\, c_{p,f}(T_{in} - T_i) \tag{4}$$

where $\dot{m}_i = \rho_f\, v_i A_i$, $c_{p,f}$ is the specific heat at constant pressure for a gas (e.g., air) or simply the specific heat for a liquid cooling fluid; ρ_f the cooling fluid density; v_i cooling fluid velocity that crosses the face of VE i; A_i the lateral face area of the VE that is crossed by the flow, and T_{in} the temperature of the cooling fluid that enters VE i. For the VE located at the wall that contains the cooling fluid input, T_{in} is the cooling fluid input temperature (e.g., external air temperature).

For Eq. (4), $\dot{m}_{fan}$ is a known parameter, based on the fan specifications or measured directly at the output orifice area in which the fan is installed. Then, a cooling flow around the equipment inside the cabinet results in all air volume elements, and v_i for each internal air VE i is estimated, based on fluid properties and VE i cross flow area, so that mass conservation is satisfied, in a way that the cooling fluid input mass flow rate is the same as the output one. Fig. 2 shows a schematic diagram of the PEBB illustrating the calculation of the cooling fluid velocity that crosses the face of VE i. Therefore, for all air VE i located at the PEBB top and bottom compartments, the result is as follows:

$$V_i = \frac{\dot{m}_{fan}/2}{\rho_f A_{free,j}} \quad (j = t \text{ or } b) \tag{5}$$

where $A_{free,j}$ is the total free cross flow area at the PEBB j compartment (top or bottom).

The model also calculates all heat transfer rates present in Eq. (1) for any instant in time. For that, the heat transfer mode is identified, and appropriate thermo-physical properties, empirical and theoretical correlations available in the technical literature are used to quantify all heat transfer rates accordingly. For assessing the complete details of the mathematical model equations, the reader is directed to the work published previously by the authors [12–14,17].

Component-level simulation incorporates thermal modeling and characterization of power electronic building blocks (PEBB) converters featuring relevant electronic components of an all-electric ship. Primary components of interest in this simulation are: inductors, capacitors, AC and DC fuses, and a tiristors/fins set as shown in Fig. 2.

3. Numerical method

The mathematical model produces a system of N (total number of volume elements) ordinary differential equations with time as the independent variable, along with the initial conditions, for the unknowns T_i, i.e., the temperatures of each volume element. Once the temperatures of each volume element are known, the corresponding relative humidity follows immediately.

The unsteady system of equations is integrated in time, from given initial conditions, explicitly using an adaptive 4th/5th order Runge–Kutta/Fehlberg method [18]. If the transient solution is of no interest, the system is solved directly for the steady-state solution. The time derivative terms in the ODE's system are dropped and a system of N nonlinear algebraic equations is obtained. In this case the unknowns are the steady-state temperatures at the center of each volume element. The resulting nonlinear system of algebraic equations is solved using a Newton–Raphson method. The system of equations is linearized with respect to the cell center temperatures, after which the volume elements' relative humidities are computed.

The convergence of the numerical results was verified by successive mesh refinements [19] and monitoring the variation of the Euclidean norm of the temperatures numerical solution in the entire domain. However, the max-norm (or infinity norm) could also be used in order to reduce computational effort. The results of a less refined mesh (mesh 1) are compared to the results of a more refined mesh (mesh 2), and the refinements stop when the mesh refinement relative error, ε_m, criterion is satisfied, then mesh 1 is selected as the converged mesh, as follows:

$$\varepsilon_m = \frac{\left|\|T\|_{m1} - \|T\|_{m2}\right|}{\|T\|_{m1}} \leq 0.01 \tag{6}$$

Both the mesh and the numerical results were processed for graphical visualization in different planes and surfaces. For that, a free graphic software produced by the Lawrence Livermore National Laboratory was utilized [15].

According to the criterion of Eq. (6), the final converged mesh utilized in the simulations performed in this study contained 2000 volume elements, as it is shown in Fig. 3. The dimensions and quantity of elements in each direction are listed in Table 1.

4. Experiments

4.1. Experimental rig

The power electronic building block used in the experiments, i.e., the controlled phase converter, was composed by tiristors of

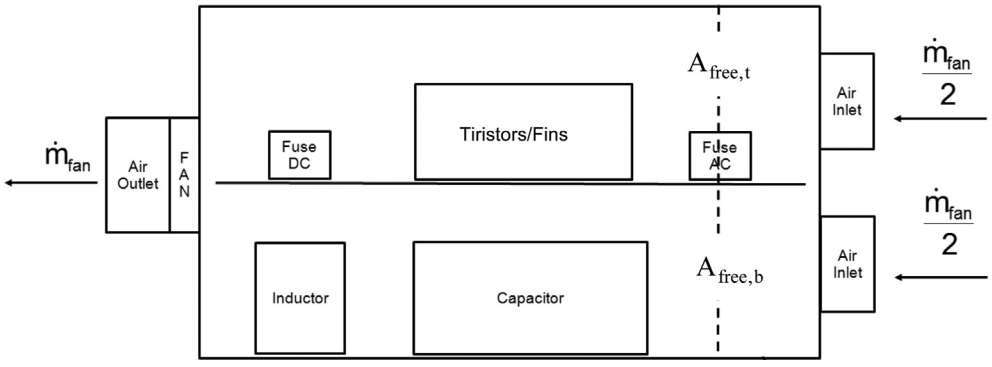

Fig. 2. The estimation of the cooling air mass flow rate throughout the PEBB around the electronic components.

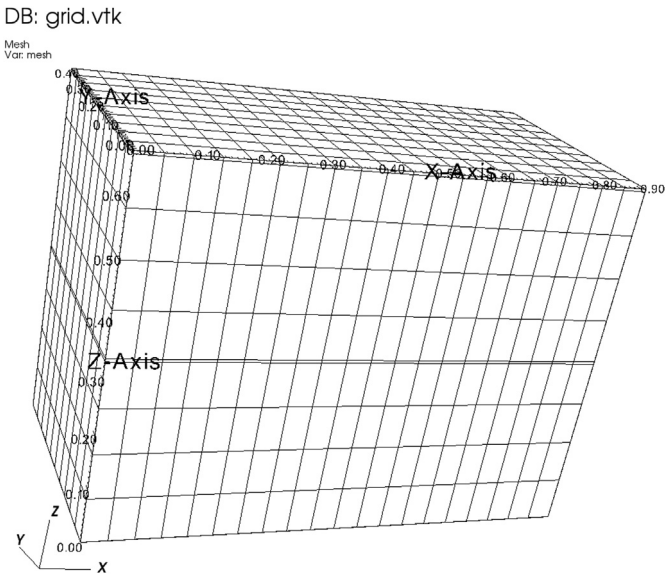

Fig. 3. PEBB converged mesh according to the criterion of Eq. (5).

150 A, capacitors, inductors and fuses. The components set was assembled in a cabinet measuring 0.91 m × 0.47 m × 0.67 m, as shown in Fig. 4(a). The system was air cooled by a fan manufactured by Dayton, model 4WT42A, with a nominal maximum air volumetric flow rate of 0.1128 $m^3\ s^{-1}$. The utilized electrical load consisted of a bank of 3 (three) electrical resistances composed, each with 4.6 Ω, which is shown in Fig. 4(b). Through the load, the PEBB generated electric power was dissipated to the environment.

A data acquisition system was assembled in the laboratory to monitor and record in files all experiments in real time, using the software *LabView 8.2*, together with data acquisition boards, i.e.: NI PXI 1010 – *Chassis*, SCXI-1102 – *Filter* 2 Hz, SCXI-1581 – *Current Source*, PXI-6251 – *Data Acquisition*, PXI-6133 – *Waveform Capture*, PXI-6251 – *Voltage Output*. The physically measured quantities were: the external air temperature, 26 PEBB temperature points, 5 electric current points, 4 voltage points.

High precision thermistors of type 44004RC, standard type Bead I, with a maximum diameter of 2.4 mm, were utilized for the temperature measurements. The thermistors were immersed in a constant temperature bath, and sixty-four temperature measurements were made at 20 °C, 30 °C, 40 °C, …, 80 °C. The largest standard deviation of these measurements was 0.0006 °C, therefore the bias limit was considered ±0.0012 °C for all the thermistors. A thermometer HH506R manufactured by Omega Inc. was used to measure the external air temperature. The complete list of the utilized instrumentation and corresponding specifications is shown in Table 2.

The 26 temperature points were selected in order to represent each analyzed component temperature and also the cabinet internal air temperature. Table 3 shows the identification number of each thermistor, the location and also the coordinates of each of them with the Cartesian referencial origin placed at the cabinet frontal inferior left corner.

Table 1
Converged mesh.

Mesh	Direction		
	L_x	L_y	L_z
Dimension (m)	0.91	0.47	0.67
Number of VE	20	10	10

The physical properties of all PEBB components are listed in Table 4. The locations and sizes of each component are listed in Table 5. The components heat generation for the two PEBB power settings is shown in Table 6.

4.2. Uncertainty analysis

The calculation of experimental uncertainties is essential for the adequate evaluation of the obtained results. Through the temperature measurements during the transient evolution of the system and at steady state conditions, it is sought to experimentally validate the numerical results obtained with the mathematical model. Such results contain uncertainties due to the measurement process and instrumentation that need to be quantified.

The average of the measurements taken in all runs with the high precision thermistors listed in Table 2, standard type Bead I, with a maximum diameter of 2.4 mm, was utilized to estimate the temperature at each point within the cabinet. The precision limit of the measurements was calculated as twice the standard deviation of the experimental runs assuming that the population follows a symmetric unimodal normal distribution, within a 95% confidence interval [20].

In this work, the temperature measurements uncertainties were estimated according to standard criteria from the American Society of Mechanical Engineers, ASME [21]. The temperature measurements uncertainties are therefore obtained as follows:

$$U_T = \sqrt{P_T^2 + B_T^2} \text{ or } \frac{U_T}{T} = \sqrt{\left(\frac{P_T}{T}\right)^2 + \left(\frac{B_T}{T}\right)^2} \tag{7}$$

where B_T is the thermistors' bias limit, and P_T the precision limit, i.e., $2\sigma_T$. Therefore, U_T is the temperature measurements uncertainty.

4.3. Experimental procedure

Two PEBB experimental tests were conducted in the laboratory. The tests were performed three times using exactly the same current and power in order to evaluate the variability of the readings and to make possible the uncertainty analysis and the construction of error bars. For the first test, the conditions consisted of a direct current of 40 A, and a voltage of 279 V which resulted in a total power to be dissipated by the bank of resistances of 11.12 kW. The second test was performed with a total power of 4.8 kW, with a voltage of 200 V and direct current of 24 A.

The test started with the PEBB in complete thermal equilibrium with the external environment, which was controlled at $T_\infty = 296 \pm 0.2$ K. The system was turned on directly to the power of 11.12 kW or 4.8 kW and the fan air volumetric flow rate was set to 0.08 $m^3\ s^{-1}$. The transient response until steady state was monitored with a 1 s sampling rate through the data acquisition system. After the test, the equipment was cooled down with fans until thermal equilibrium with the environment was achieved. The procedure was repeated three times.

5. Results and discussion

In this section, the PEBB behavior is studied experimentally and numerically. First, the measured PEBB transient and steady state thermal response is analyzed. Then, the experimental measurements are used to experimentally validate the numerical results obtained with the mathematical model presented in section 2, using 2 (two) different sets of measured data obtained for the PEBB shown in Fig. 4(a) for two different power settings. The procedure

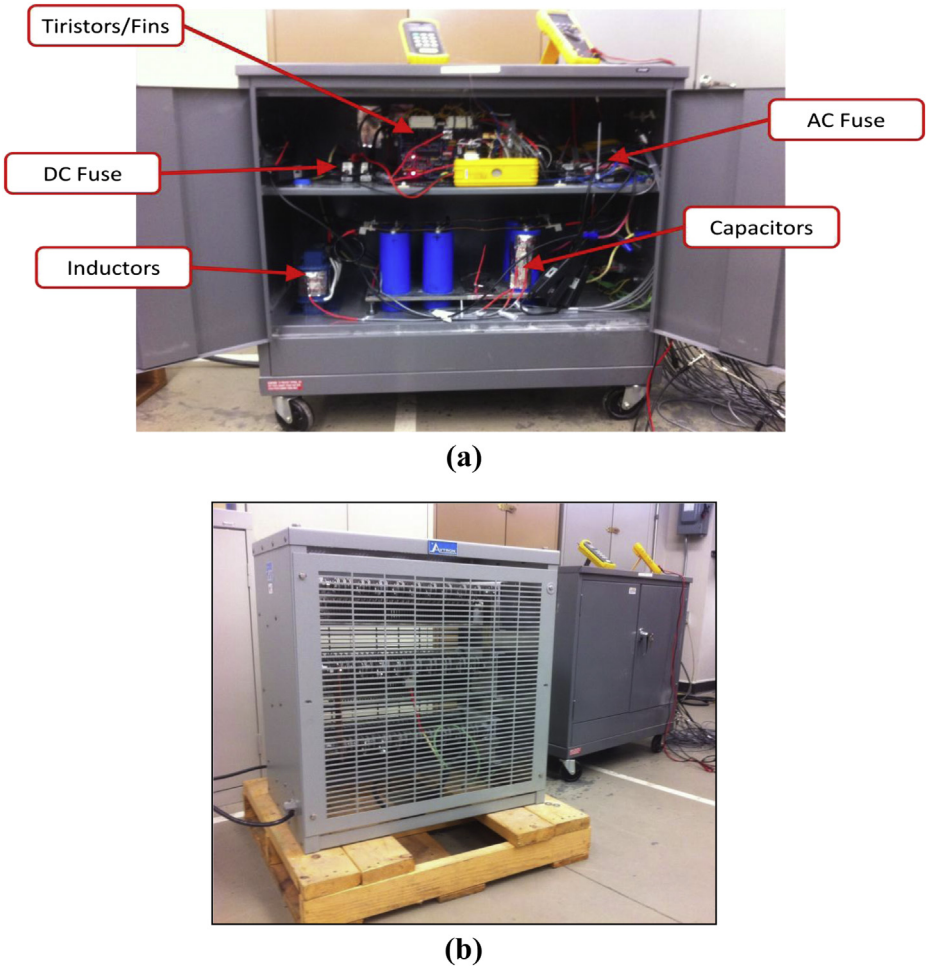

Fig. 4. PEBB with component descriptions (a), and bank of electrical resistances used as electrical load (b).

consists of solving the inverse problem of parameters estimation to verify and adjust, if necessary, estimated equivalent densities, specific heats, heat transfer surfaces, or thermal conductivities for the components, therefore adjusting the mathematical model using one PEBB power setting data, i.e., 4.8 kW. After that, the conditions corresponding to the other data set, i.e., 11.12 kW are computationally simulated with the adjusted model to verify the agreement between numerical and experimental results. Finally, the experimentally validated model is used to investigate the system global thermal conductance.

5.1. PEBB transient and steady state experimental thermal response

The analysis performed in this item is conducted with the 11.12 kW PEBB power setting. The PEBB initial condition varied slightly in the 3 runs, i.e., between 296 and 297 K.

Table 2
Instruments and sensors used for data acquisition with respective bias limits.

Instrument/sensor	Manufacturer	Model	Bias limit
Voltmeter	Probe Master	4232	2%
Voltmeter	Lecroy	AP031	2%
Multimeter	Fluke	179	0.09%
Thermometer	Omega	HH506R	0.05%
Thermistors	Measurement Specialties	44004RC	0.001 °C
Air flow meter	Fluke	922	2.5%

Table 3
Thermistors list, components and positions.

Thermistor number	Component	Position (cm) (x, y, z)
1	Capacitor – pos. 1	(58,17,9)
2	Capacitor – pos. 2	(59,16,15)
3	Capacitor – pos. 3	(62,15,18)
4	Capacitor 2	(26,28,17)
5	Air – inferior compartment pos. 1	(53,24,18)
6	Air – fan outlet	(5,21,46)
7	DC fuse	(18,29,40)
8	DC cable	(19,16,38)
9	Capacitor pos. 4	(35,38,41)
10	Resistor	(35,38,47)
11	Inductor – pos. 1	(48,16,42)
12	Transformer	–
13	Fins – pos. 1	(32,30,49)
14	Fins – pos. 2	(52,27,49)
15	Fins – pos. 3	(59,26,49)
16	AC cable L3	(69,33,47)
17	AC fuse L3	(80,22,40)
18	Internal wall	(27,46,48)
19	Air inlet	(91,24,46)
20	Not used	–
21	External wall	(33,47,49)
22	Tiristors bridge	(47,29,52)
23	Inductor – pos. 2	(10,11,9)
24	Air – inferior compartment pos. 1	(79,24,22)
25	Air – superior compartment pos. 1	(78,28,50)
26	Air – superior compartment pos. 2	(17,19,53)

Table 4
Components physical properties.

Component	Quantity	Volume (m^3)	Mass (kg)	Surface area (m^2)	Material
Tiristors/fins	1	0.00204	5.526	0.735	100% Al
AC fuse	3	3.0e-5	0.108	0.0059	Sn alloy
DC fuse	2	3.7e-5	0.108	0.0068	Sn alloy
Capacitor	6	0.00099	1.748	0.0615	60% Al, 10% PVC, 30% air
Inductor	1	0.00512	14.00	0.1581	60% Cu, 40% Fe

The representative temperature of a particular component and internal air was defined as the arithmetic mean of all temperature measurements obtained from the thermistors installed in the component or internal air (4 thermistors). In this way, an instantaneous mean temperature was available for each component and the internal air. The measured temperatures time evolution is shown in Fig. 5, and the plotted curves are also the arithmetic mean of the three test runs.

Fig. 5(a) shows the measured transient mean temperature evolution for the tiristors/fins set, AC fuse, inductor, capacitors, and DC fuse. The inductor is the component that presents the largest thermal inertia within the PEBB taking more time to reach steady state conditions. The transient evolution lasted approximately 4000 s until steady state was achieved.

According to Table 3, the cabinet internal air temperature was measured with 4 thermistors. Two thermistors measured the air input and output (fan) temperatures. Then, the temperature difference between the input and output allowed for the calculation of the heat transfer rate collected by the air stream. Two thermistors measured the cabinet wall internal and internal side temperatures. Fig. 5(b) shows the transient evolution of the internal air mean, input and output air temperatures, and the wall temperatures as well. All temperatures stabilized approximately around 2000 s.

Additionally, the software VisIt [15] was used to generate the components and internal air temperature visualization. The mesh was the same as the one used for the numerical simulations, as described in Section 3. Fig. 6(a) shows the resulting measured internal temperature distribution at the cabinet midplane for steady state conditions. Note that the distribution of the heat generating components is consistent with the actual components distribution shown in Fig. 4(a), and is revealed by the higher temperature regions, except for the capacitors which present low heat generation, therefore their temperature is almost the same as the cabinet internal air temperature.

5.2. Experimental model adjustment and validation

5.2.1. Model adjustment

A computational code was written in Fortran language based on the numerical method described in section 3 to obtain the solution to the mathematical model presented in Section 2, i.e., PEBB internal air and components temperatures. The input parameters are the PEBB geometric features, components heat generation and physical properties. The geometry and several physical properties were measured directly from the PEBB prototype, and are listed in Tables 1 and 4–6. The PEBB initial condition for the simulations was set as 296.3 K.

Table 5
Components dimensions and position.

Component	Position (m)			Dimension (m)		
	x	y	z	L_x	L_y	L_z
Tiristors/fins	0.3	0.2	0.35	0.3	0.2	0.2
AC fuse	0.7	0.2	0.35	0.08	0.05	0.05
DC fuse	0.1	0.2	0.35	0.08	0.05	0.05
Capacitor	0.3	0.2	0.05	0.4	0.3	0.2
Inductor	0.7	0.2	0.35	0.1	0.05	0.05

Table 6
Components heat generation.

Component	Test 1 (200 V; 24 A; 4.8 kW) $\dot{Q}_{gen}$ (W)	Test 2 (279 V; 40 A; 11.12 kW) $\dot{Q}_{gen}$ (W)
Tiristors/fins	130	182
AC fuse	8.7	11.5
DC fuse	3	7.7
Capacitor	0	0
Inductor	23	60
Total	**164.7**	**261.2**

The information on the composition of all components listed in Table 4 is used to estimate equivalent densities, specific heats, and thermal conductivities, and heat transfer surfaces ratios for the components, as follows:

$$\rho_{eq} = \frac{V_R}{V_m}\rho_R;\ c_{eq} = \frac{\sum_{i=1}^{n} m_i c_i}{m_{co}};\ k_{eq} = \left(\frac{V_R}{V_m}\right)^{1/3} k_R;\ \gamma = \frac{S_R}{S_m} \tag{8}$$

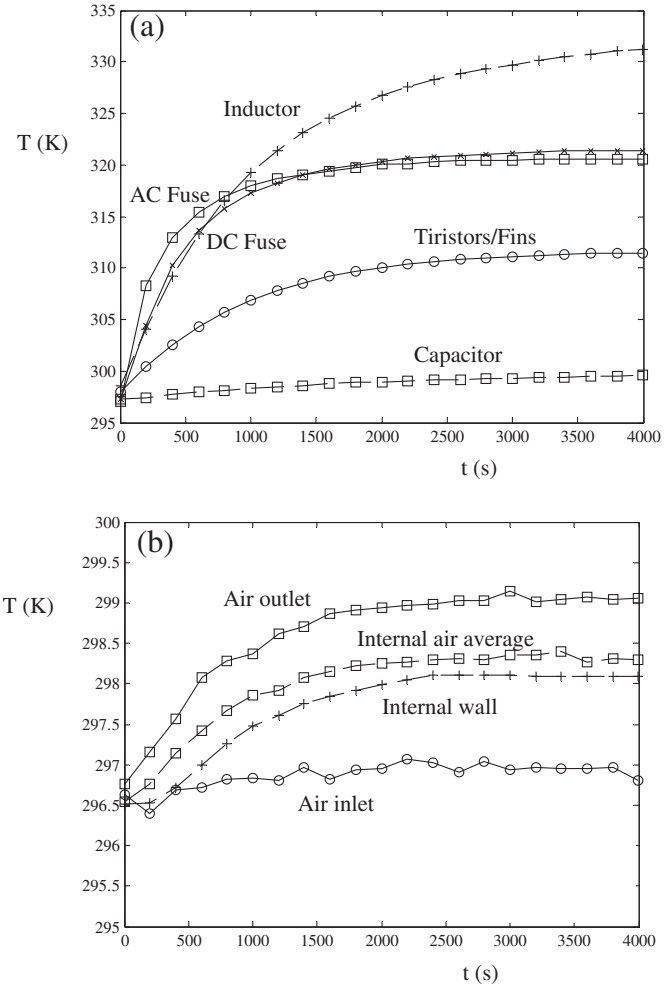

Fig. 5. Experimental thermal response of the 11.12 kW PEBB power setting: (a) measured components transient mean temperature evolution, and (b) measured input, output, average internal air, and wall transient temperature evolution.

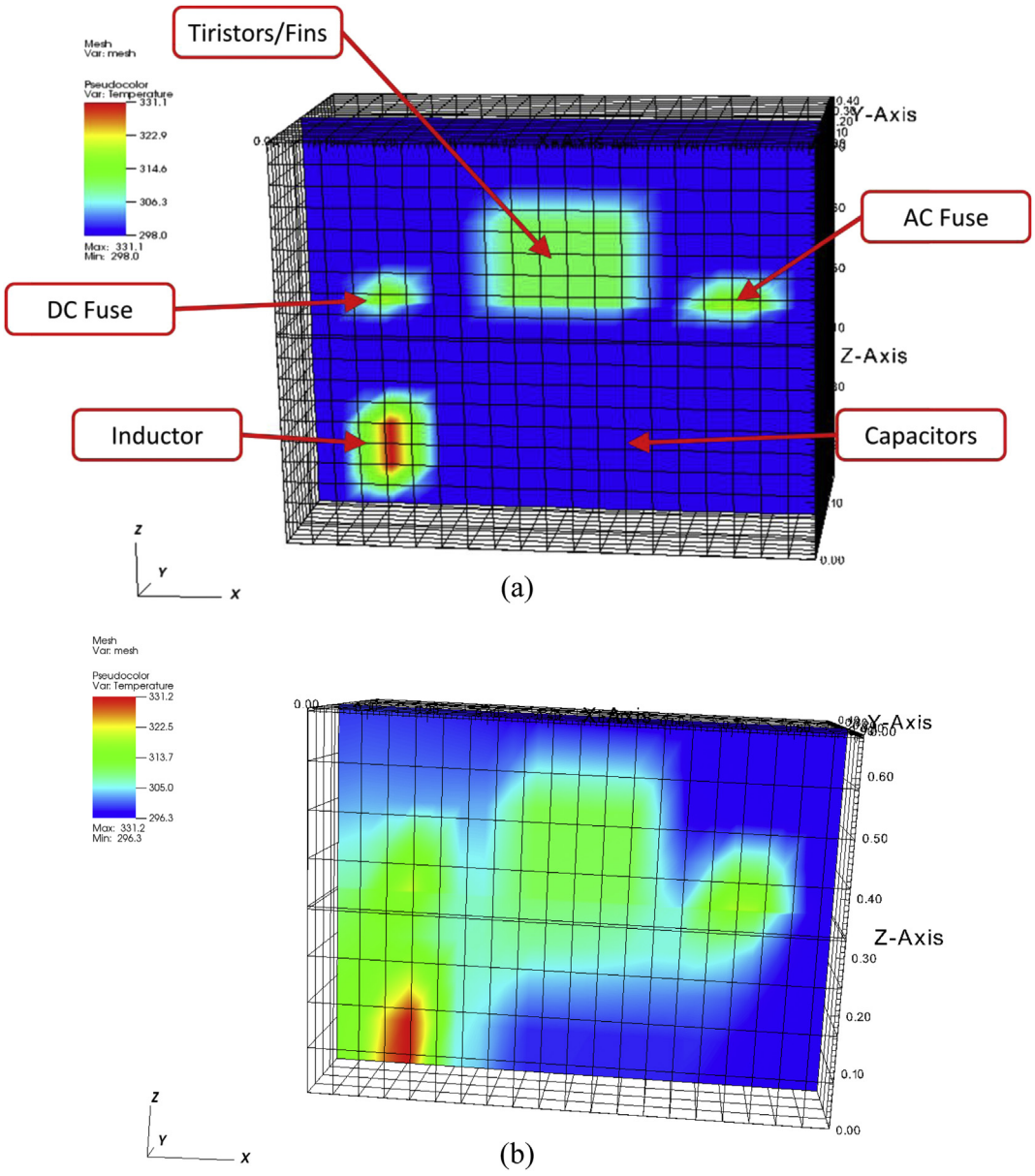

Fig. 6. Thermal response of the 11.12 kW PEBB power setting: (a) measured components temperature distribution visualization at steady state, and (b) simulated components temperature distribution visualization at steady state.

where ρ_R is the actual component weighed average density; V_R/V_m the ratio between the component actual and mesh volume; m_i the mass of material i in the component, which is composed by n material types; m_{co} the component mass; k_R is the actual component weighed average thermal conductivity, and $\gamma = S_R/S_m$ the ratio between the component actual and mesh heat transfer surface.

The model adjustment was performed with the 4.8 kW PEBB power setting. The model adjustment procedure consisted of solving the inverse problem of parameter estimation (IPPE) [22], using the mathematical model, i.e., by turning a variable into a parameter, and vice-versa. For that, what was originally a variable is imposed to the model as an input parameter. In this study, the variables available from the experiments were the measured temperatures of the PEBB prototype. Therefore, as many as 24 measured parameters (corresponding to the internally measured temperatures) could become variables in the model, according to Table 3.

The procedure started by selecting the parameters to become the variables to be determined. According to Eq. (8), equivalent densities, specific heats, and thermal conductivities could be estimated appropriately. However, although heat transfer surfaces ratios, γ, could be accessed, the uncertainty in the direct measurements was high. Therefore, the 5 internal components heat transfer surfaces ratios, were the selected parameters to be adjusted by the IPPE. The numerical solution of the IPPE was obtained for the steady state with the 4.8 kW power setting, and the 5 measured average temperatures at each component were used as inputs to the mathematical model, which calculated the 5 internal components heat transfer surfaces ratios, using as initial guesses the measured ones. As a result, using the calculated γ, the 5 components average temperatures predicted by the mathematical model, matched the measured ones. The results are shown in Table 7, which also shows the measured components actual volume to mesh volume ratios required by Eq. (8).

Table 7
Volume and heat transfer surface correction values.

Component	Number of volume elements	V_R/V_m	γ (IPPE)
Tiristors/fins	90	0.755	1.940
AC fuse	3	0.472	0.410
DC fuse	2	0.566	0.437
Capacitor	96	1.417	0.882
Inductor	16	1.417	1.248

5.2.2. Model experimental validation

After performing the model adjustment, the next step was the model experimental validation, which was performed with the 11.12 kW PEBB power setting. The calculated γ values were then used as input to the mathematical model in order to obtain numerically the PEBB internal temperature distribution. The PEBB initial condition for the simulations was set as 296.3 K.

Fig. 6(b) shows the numerically simulated temperature distribution obtained with the adjusted model for temperatures at each VE, which compares qualitatively well with the experimentally obtained temperature distribution, in which it should be noted that average temperatures are represented both for the 5 components and internal air, therefore a quantitative match of the results was not expected, but the comparison is shown in order to observe the resulting similar trends. However, the maximum measured temperature was 331.1 K whereas the maximum calculated one was 331.2 K as it is observed in the legends of Fig. 6(a) and (b), which are in very good agreement.

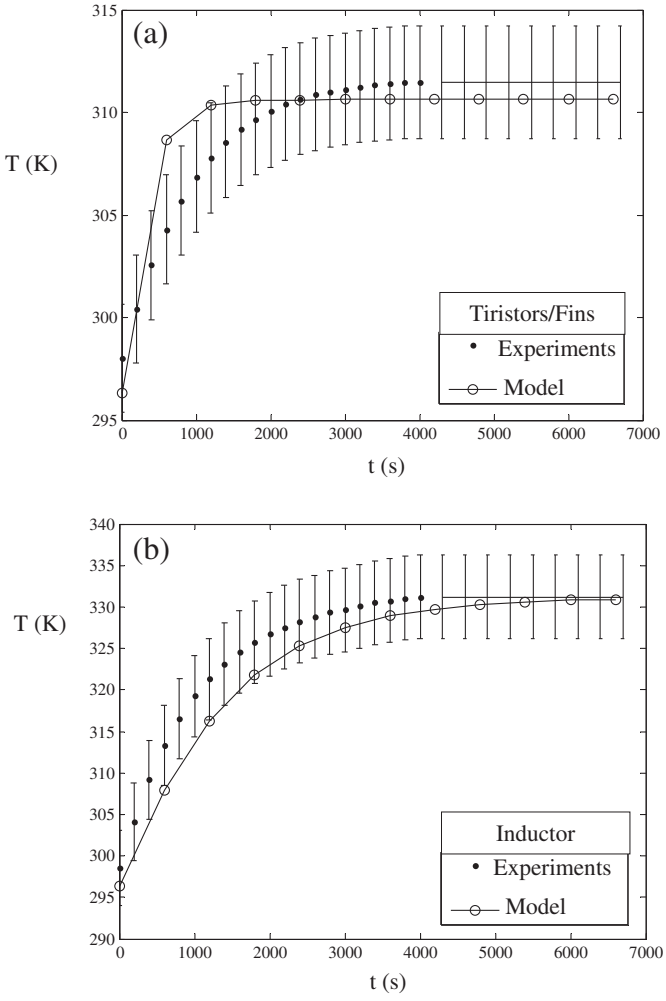

Fig. 7. Comparison between experiments and simulation curves for the 11.12 kW PEBB power setting for the average temperature transient evolution to steady state: (a) tiristors/fins set, and (b) inductor.

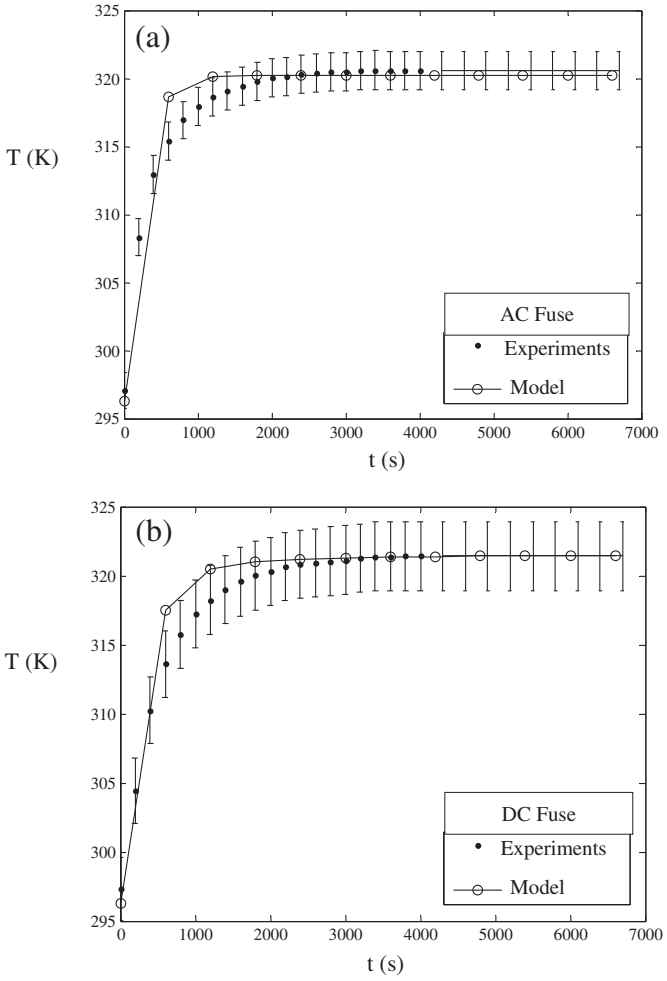

Fig. 8. Comparison between experiments and simulation curves for the 11.12 kW PEBB power setting for the average temperature transient evolution to steady state: (a) AC fuse, and (b) DC fuse.

In order to investigate more deeply the accuracy of the numerical predictions of the adjusted model in comparison to the collected experimental data for the PEBB 11.12 kW setting, Figs. 7–10 provide simulation and experimental results for the average temperatures of the 5 components and 3 selected internal air locations. In the experimental results the uncertainties were calculated according to Eq. (7), and the largest observed value for U_T/T during the transient to steady state evolution of the measurements was used to calculate the error bars shown in all experimental points for consistency.

In Fig. 7(a), it is shown that for the tiristors/fins set the simulated temperature curves lie within the error bars for the steady state and evolve at a higher rate during the transient, but mostly remaining within the margin of error. This is probably due to a slight underestimation of the total inertia (mass) of the tiristors/fins set. A similar phenomenon was observed for the inductor, as the results of Fig. 7(b) show, but in this case inductor inertia must have been slightly overestimated. These two components are the ones that generate most heat in the PEBB, therefore it is considered that the

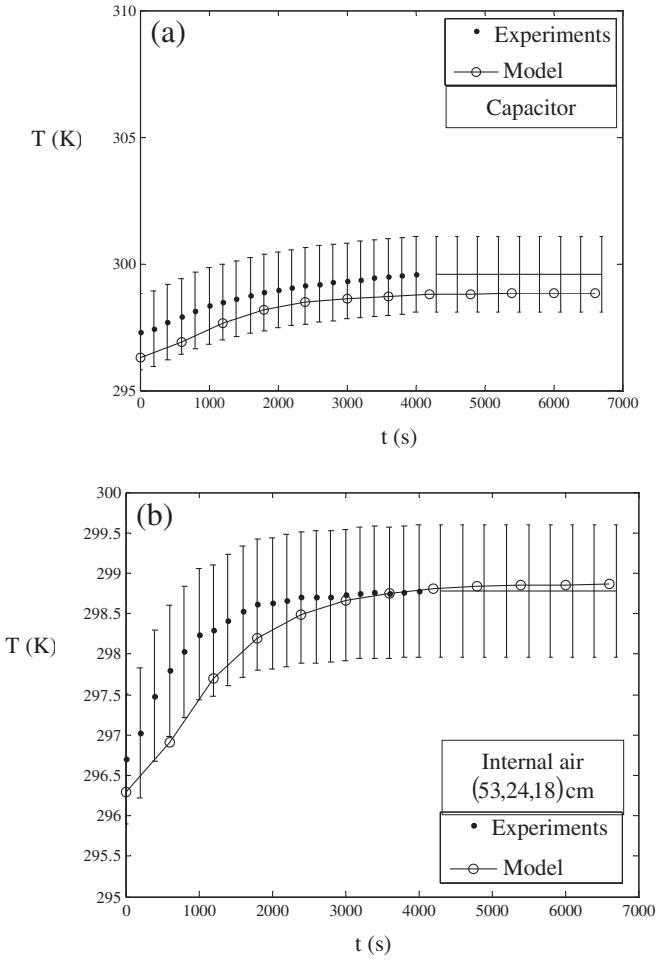

Fig. 9. Comparison between experiments and simulation curves for the 11.12 kW PEBB power setting for the average temperature transient evolution to steady state: (a) capacitor, and (b) internal air at position (53,24,18) cm.

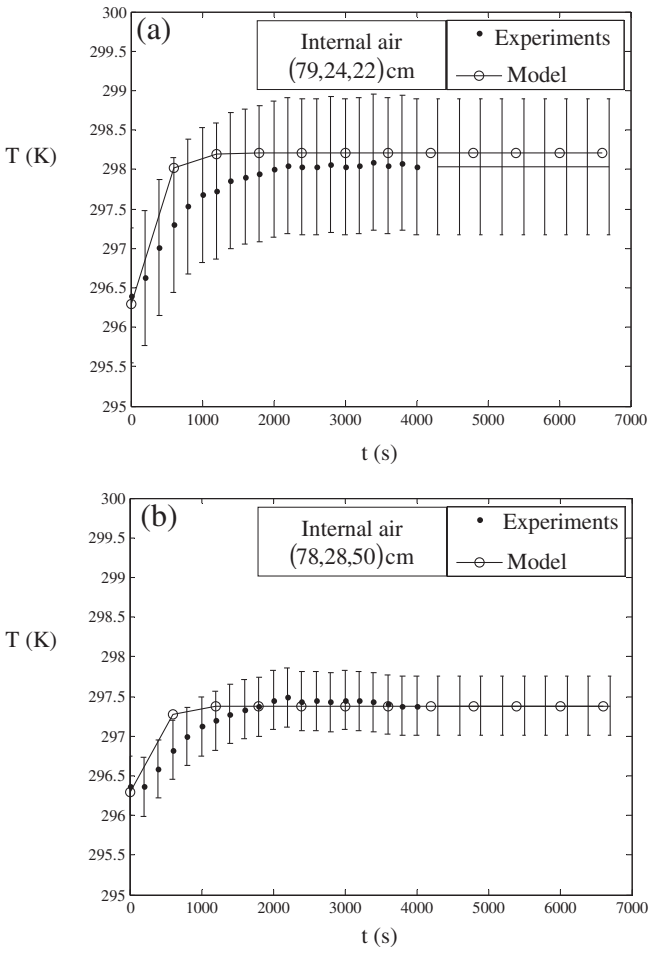

Fig. 10. Comparison between experiments and simulation curves for the 11.12 kW PEBB power setting for the average temperature transient evolution to steady state: (a) internal air at position (79,24,22) cm, and (b) internal air at position (78,28,50) cm.

simulated and experimental curves are in very good qualitative and quantitative agreement, mainly if the analysis prioritizes the assessment to steady state conditions. Fig. 8(a) and (b) allows for drawing similar conclusions, in this case with respect to the thermal response of the AC and DC fuses. Due to a significantly lower heat generation than the other components and an accurate inertia estimation, the capacitors simulated and experimental curves agreed both in slope and in absolute values for all points, as it is shown in Fig. 9(a).

The simulated and experimental temperatures for the internal air at 3 different locations in the PEBB are shown in Figs. 9(b), 10(a) and (b). All predicted temperature values lie within the error bars for the transient to steady state evolution in the 3 locations. Therefore, these results test and validate the assumptions made to write Eq. (4) that predicts the convection heat transfer rate extracted by the fan driven air stream that flows across the PEBB, i.e., an approximate air flow field is capable of allowing the simplified mathematical model to produce accurate thermal predictions.

5.3. PEBB simulation

In order to illustrate the application of the experimentally validated PEBB mathematical model, the thermal response of the PEBB is assessed through its thermal conductance, which is defined as follows:

$$\mathrm{UA} = \frac{\dot{Q}_{\mathrm{gen,tot}}}{T_{\mathrm{air,avg}} - T_{\infty}} \tag{9}$$

The numerical simulations were conducted for $\dot{Q}_{\mathrm{gen,tot}} = 164.7$ W and 261.2 W, starting with the initial condition $T_0 = 296.3$ K which was set higher than the controlled external air temperature $T_{\infty} = 296$ K. The reason is that in the experiments, the PEBB initial condition varied slightly in the 3 runs, i.e., between 296 and 297 K. Therefore, in Fig. 11, it is seen that UA starts at $t = 0$ s with a finite value. If the PEBB were in perfect thermal equilibrium with the environment, then $\mathrm{UA} \to \infty$, since in the denominator of Eq. (9), $\Delta T = T_0 - T_{\infty} = 0$ K. Note that, for the first PEBB power setting, i.e., $\dot{Q}_{\mathrm{gen,tot}} = 164.7$ W, UA is higher than for the second one, i.e., $\dot{Q}_{\mathrm{gen,tot}} = 261.2$ W, in the beginning of the simulation, since for higher power dissipation the air internal temperature increases faster than at a lower power dissipation. However, as the system evolves in time this trend is inverted at around $t = 1300$ s, since the cabinet is capable of rejecting more heat with $\dot{Q}_{\mathrm{gen,tot}} = 261.2$ W than at $\dot{Q}_{\mathrm{gen,tot}} = 164.7$ W. Another way of seeing the importance of assessing UA for electronic packaging is by noting that at the highest possible UA, the electronic equipment will operate at the minimum possible temperature that should be

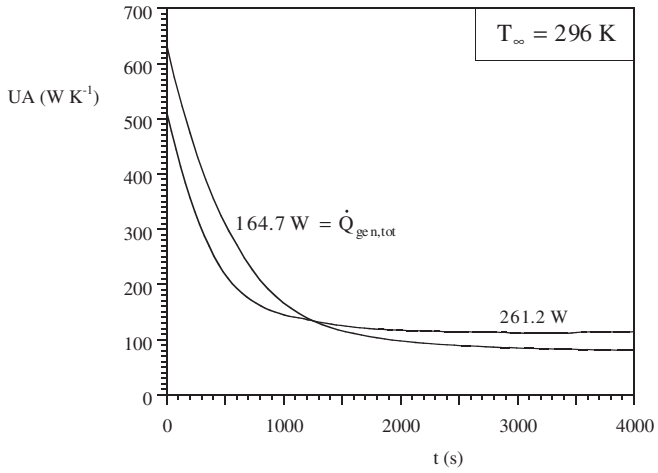

Fig. 11. The effect of total heat generation on PEBB thermal conductance.

below a given ceiling operating temperature, which also determines the maximum possible $\dot{Q}_{gen,tot}$ for the cabinet. This analysis stresses the importance of a transient simulation for performance assessment in PEBB control, design and optimization, which will depend on the expected PEBB operation regime, i.e., whether it is under transient loading or at steady state.

Finally, as an example of the model application in a transient simulation, a transient analysis is conducted numerically with the model. Fig. 12 shows the thermal transient response of the PEBB when the total heat generation mode changes from $\dot{Q}_{gen,tot} = 164.7$ W to $\dot{Q}_{gen,tot} = 261.2$ W, then back to $\dot{Q}_{gen,tot} = 164.7$ W, and finally goes up to $\dot{Q}_{gen,tot} = 391.8$ W, which is a load 50% higher than $\dot{Q}_{gen,tot} = 261.2$ W. The total simulation time was close to 20,000 s. Besides information on the time required to achieve new steady state conditions, the results demonstrate that the components temperature vary significantly from one heating mode to another, an effect that becomes increasingly important as total heat generation increases, whereas internal air average temperature varies only slightly for all heating modes. This is explained by the fact that air has a low thermal conductivity and therefore poor thermal contact with the components. Such effect is commonly disregarded in current electronic packaging practice which usually specifies operating conditions for components based on internal air average temperature. Therefore, in spite of low internal air average temperature, the procedure could lead to component failure as the total heat generation increases, as the present model demonstrates.

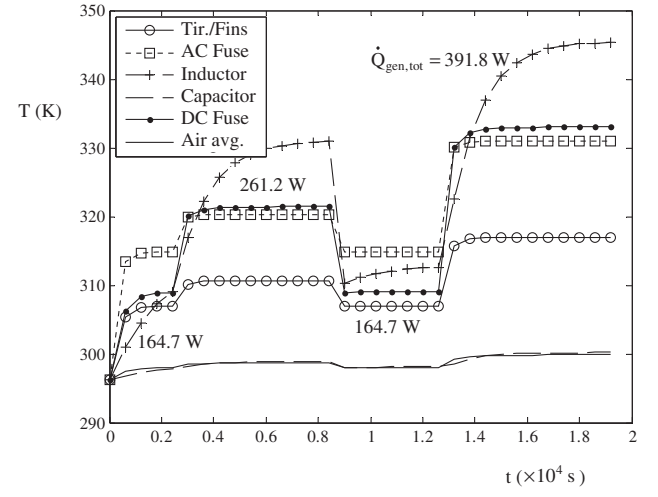

Fig. 12. The effect of the transient change of total heat generation mode on PEBB thermal response.

6. Conclusion

In this paper, a general transient mathematical model for the thermal management of physical systems with heat sinks and sources (vemESRDC) previously developed by the authors was experimentally validated by direct comparison of power electronic building block (PEBB) temperature measurements to model numerical predictions with good quantitative and qualitative agreement. For that, the model was first adjusted by the solution of the inverse problem of parameter estimation (IPPE) to obtain appropriate equipment heat transfer surfaces ratios, with a 4.8 kW PEBB power setting, followed by the use of a 11.12 kW PEBB power setting for the experimental validation of the adjusted model. Hence, the model could be reliably used to simulate and analyze the PEBB thermal response under different geometric and operating conditions. Such analyses are capable of providing optimal components distributions and settings for maximum global performance (e.g., size reduction, increased power settings).

In order to illustrate the importance of transient analyses for electronic packages thermal management, the experimentally validated model was used to assess PEBB performance through the system thermal conductance transient evolution to steady state. The results demonstrated that for any given cabinet geometry, no matter how complex the actual design might be, a maximum possible $\dot{Q}_{gen,tot}$ for the cabinet could be estimated through numerical simulations, so that the electronic equipment will operate below a specified ceiling internal air temperature. Furthermore, transient simulations demonstrate that the components temperature vary significantly from one heating mode to another, whereas internal air average temperature varies only slightly for all heating modes, therefore not only average internal air temperature should be monitored for preserving equipment functionality.

The model allows for the use of a relatively coarse mesh to discretize the domain and still obtain converged numerical results, with low computational time, in spite of the diverse nature of the components inside the domain. Therefore, the vemESRDC application is expected to be an efficient tool for the thermal management of heat generating packages (e.g., PEBB, future all-electric ship).

Acknowledgements

This work was supported through the Office of Naval Research (ONR) grant – N00014-08-1-0080.

References

[1] B. Wagner, All-electric ship could begin to take shape by 2012, NDIA's Business and Technologies Magazine (November 2007).
[2] R.R. Soman, E.M. Davidson, S.D.J. McArthur, Using functional failure mode and effects analysis to design the monitoring and diagnostics architecture for the zonal MVDC shipboard power system, in: IEEE Electric Ship Technologies Symposium, 2009, pp. 123–128. Baltimore, Maryland, USA.
[3] S.S. Jogwar, M. Baldea, P. Daoutidis, Tight energy integration: dynamic impact and control advantages, Computers & Chemical Engineering 34 (9) (2010) 1457–1466.
[4] S. Mustafiz, M.R. Islam, State-of-the-art petroleum reservoir simulation, Petroleum Science and Technology 26 (10–11) (2008) 1303–1329.
[5] P. Lall, M.N. Islam, M.K. Rahim, J.C. Suhling, Prognostics and health management of electronic packaging, IEEE Transactions on Components and Packaging Technologies 29 (3) (2006) 666–677.
[6] P. Lall, M. Hande, C. Bhat, J. Lee, Prognostics health monitoring (PHM) for prior damage assessment in electronics equipment under thermo-mechanical

loads, IEEE Transactions on Components Packaging and Manufacturing Technology 1 (11) (2011) 1774–1789.
[7] N. Gnanasambandam, A. Primavera, K. Srihari, The reliability prediction of electronic packages – an expert systems approach, International Journal of Advanced Manufacturing Technology 27 (3–4) (2005) 381–391.
[8] P.E. Bagnoli, C. Padovani, A. Pagni, G. Pasquinelli, A thermomechanical solver for multilayer power electronic assemblies integrated into the DJOSER thermal simulator, Journal of Electronic Packaging 133 (1) (2011). Art. No.: 011005.
[9] P. Yang, Z.X. Chen, Testing on dynamic behavior of PBGA assembly by considering fixed-modes, Microelectronics International 28 (2) (2011) 23–29.
[10] B. Shapiro, Creating compact models of complex electronic systems: an overview and suggested use of existing model reduction and experimental system identification tools, IEEE Transactions on Components and Packaging Technologies 26 (1) (2003) 165–172.
[11] J.V.C. Vargas, G. Stanescu, R. Florea, M.C. Campos, A numerical model to predict the thermal and psychrometric response of electronic packages, ASME Journal of Electronic Packaging 123 (3) (2001) 200–210.
[12] J.C. Ordonez, J.V.C. Vargas, R. Hovsapian, Modeling and simulation of the thermal and psychrometric transient response of all-electric ships, internal compartments and cabinets, Simulation 84 (8–9) (2008) 427–439.
[13] F.G. Dias, J.A. Souza, J.C. Ordonez, J.V.C. Vargas, R. Hovsapian, J.V. Amy Jr., Notional all-electric ship thermal simulation and visualization, in: Proceedings of the 2009 IEEE Electric Ship Technologies Symposium, Baltimore, Maryland, ESTS Proceedings, IEEE, New York, 2009.
[14] J.V.C. Vargas, J.A. Souza, R. Hovsapian, J.C. Ordonez, T. Chiocchio, J. Chalfant, C. Chryssostomidis, E. Dilay, Notional all-electric ship systems integration thermal simulation and visualization, Simulation 88 (9) (2012) 1116–1128.
[15] VisIt 1.11.1 Manual, Lawrence Livermore National Laboratory, Livermore, CA, USA, 2008.
[16] J.A. Souza, F.M. O'Lary, R. Hovsapian, J.C. Ordonez, J.V.C. Vargas, J. Chalfant, Visualization tool for notional all-electric ships data bases, in: Proceedings of the 2010 Grand Challenges in Modeling and Simulation, Ottawa, Canada, GCMS Proceedings, July 11–14, 2010.
[17] E. Dilay, J.V.C. Vargas, J.C. Ordonez, R. Hovsapian, J. Chalfant, C. Chryssostomidis, A mesh generation strategy for representing hull geometry in ESRDC ship thermal simulation and visualization, in: Proceedings of the 2012 Grand Challenge in Modeling and Simulation, Genoa, Italy, GCMS Proceedings, July 8–11, 2012.
[18] D. Kincaid, W. Cheney, Numerical Analysis, Wadsworth, 1991.
[19] Editorial Journal of heat transfer editorial policy statement on numerical accuracy, ASME Journal of Heat Transfer 116 (1994) 797–798.
[20] S. Lipschutz, M.L. Lipson, Theory and Problems of Probability, second ed., McGraw-Hill, New York, 2000.
[21] J.H. Kim, T.W. Simon, R. Viskanta, Journal of heat transfer policy on reporting uncertainties in experimental measurements and results [editorial], Journal of Heat Transfer 115 (1993) 5–6.
[22] W.J. Minkowycz, E.M. Sparrow, G.E. Schneider, R.H. Pletcher, Handbook of Numerical Heat Transfer, second ed., Wiley, New York, 2006 (Chapter 17).